






Using acoustic emission for condition monitoring of the main shaft bearings in 4-point suspension wind turbine drivetrains

Housam Mohammad ^a, Frantisek Vlastic ^a, Jiri Zacek ^a, Baraah Maya ^b
and Pavel Mazal ^a

^aInstitute of Machine and Industrial Design, Brno University of Technology, Brno, Czechia; ^bInstitute of mathematics, Brno University of Technology, Brno, Czechia

ABSTRACT

The continuous growth of wind power technology makes condition monitoring of wind turbine components crucially important for their operational efficiency. The main shaft bearings in wind turbines have been identified as one of the most critical components in the system, especially with the ongoing increase in rotor size and weight. This increase made the 4-point suspension drivetrain more preferable. In this study, we present a novel approach for condition monitoring of the main shaft bearings in a 2 Megawatt wind turbine with 4-point suspension drivetrain using primarily acoustic emission (AE). The focus was on the analysis of time and frequency domains of the AE signal, where the dominant frequency of each AE hit was identified and plotted back in the time domain to create the so-called dominant frequency map in specific time intervals for each bearing. A comparison between the two dominant frequency maps of the two bearings gives valuable insights into the condition of the two bearings. The distinctive nature of the dominant frequency bands in the dominant frequency maps presented promising potential for this method. The presented method is straightforward and can be automated and then integrated into a planned predictive maintenance programme for this wind turbine.

ARTICLE HISTORY

Received 6 August 2023

Accepted 5 November 2023

KEYWORDS

Acoustic emission (AE); wind turbine (WT); main shaft bearing; condition monitoring (CM); dominant frequency (DF)

1. Introduction

With the rise of green energy, wind power has become the fastest-developing renewable energy in the world. As the Global Wind Report [1] shows, 2022 was another record year for wind installations and particularly for the fast-growing offshore wind sector. However, the report also points out that new installations must still quadruple by the end of this decade to achieve the goal of net zero emissions by 2050. The total global wind power capacity is now up to 837 GW, helping the world avoid over 1.2 billion tons of CO₂ annually [1].

The efficient operation of WTs heavily relies on the reliable performance of their critical components. Any failure of these components can lead to downtime and

CONTACT Housam Mohammad  Housam.mohammad@vutbr.cz

© 2023 The Author(s). Published by Informa UK Limited, trading as Taylor & Francis Group.

This is an Open Access article distributed under the terms of the Creative Commons Attribution License (<http://creativecommons.org/licenses/by/4.0/>), which permits unrestricted use, distribution, and reproduction in any medium, provided the original work is properly cited. The terms on which this article has been published allow the posting of the Accepted Manuscript in a repository by the author(s) or with their consent.

maintenance costs, affecting the energy production efficiency. Bearings are considered to be one of the most critical components in any WT. Therefore, the timely detection of bearing conditions is very important for the optimal functioning of WTs. The failure of the main shaft bearings is one of the costliest operations. It may not happen as frequently as the failure of the gearbox bearings [2,3], as shown in Figure 1, but when it happens, it is more complicated. Moreover, looking at the research literature, we notice that CM of the main shaft bearings has not received similar attention as the CM of gearbox bearings in WTs, which is one of our main motivations for conducting this research.

De Azevedo et al. concluded in a review study [4] that the WT bearings should be monitored due to their high impact on downtime. They also summarised the challenges of CM systems and emphasised that there should be more papers describing the practical challenges and aspects of CM system methodologies to make implementations on wind farms easier and faster.

An AE-based method for CM of low-speed slew bearing was presented in another review paper by Caesarendra et al. [5]. The authors reviewed the use of AE on rolling element bearings and concluded that few work has been done on the application of AE for very low-speed bearings with naturally occurring damage. From their experimental study on low-speed slew bearing, they concluded that counts, energy, duration, amplitude, ASL (average signal level) and RMS (root mean square) effectively identify significant changes in the bearing condition. They proposed a feature extraction method for the AE waveform signal using the LLE algorithm (Largest Lyapunov Exponent), then demonstrated that the LLE feature can detect the sign of failure earlier than the AE hit parameters. LLE has been applied to the vibration signal of low-speed slew bearings in another study [6] by Caesarendra et al., where the feature extraction has been explained in more details. The more samples used for the LLE input, the more accurate the results, but this requires more computation time. Since AE is sampled at high sampling rates, minimum samples for LLE input were necessary.

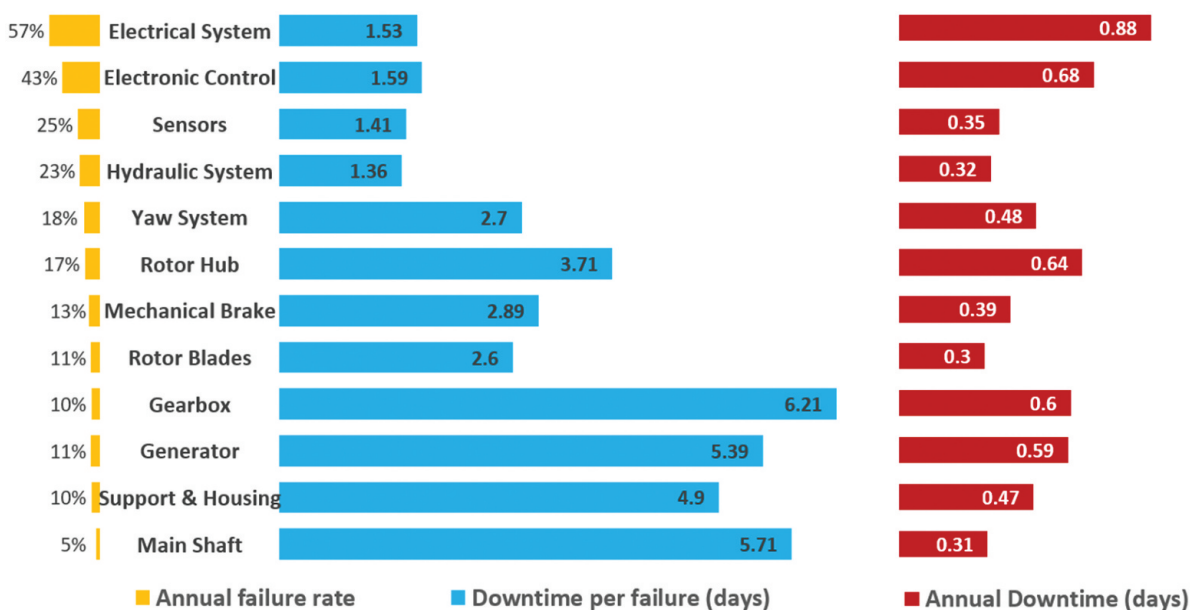


Figure 1. Failure rates and downtimes for different subassemblies from WTs [2,3].

In a commendable effort, Z. Liu and L. Zhang [7] reviewed the current CM & Fault Diagnosis (FD) achievements of large-scale WT bearings and they compared different research cases. In their concluding remarks, they mentioned the lack of research on the diagnosis of slow speed bearings. They distinctly concluded that most of the existing works on failure mode assessment of large-scale WT bearings were only validated with artificially seeded defects in idealised laboratory environments. Therefore, they suggested more reliable CM & FD methods and more evaluation of the diagnosis methods in field tests. In our research, we worked in accordance with these recommendations precisely.

In a review paper of CM techniques of WT main bearings, Gbshi S. et al. [8,9] summarised the strengths and limitations of all the available CM methods. They recommended effective noise suppression algorithms and advanced signal-processing methods for discriminating vibration fault features in low frequency rotating components such as the WT main bearings. The authors also concluded that studies investigating modern techniques are very sparse in the literature. Therefore, more studies should be considered in this direction.

Zhipeng M. et al. [10] introduced an integrated monitoring scheme for the WT main bearings using AE. It is proposed for low-speed bearing fault diagnosis, where they developed a rotating speed estimation approach to specify the exact r.p.m., which is estimated from the AE signal itself. Then they constructed a model for what they called effective damage localisation to improve maintenance efficiency in practical applications. The authors concluded that their model is able to detect the incipient damage as well as determine the damage location, which will greatly improve the health management efficiency of the main bearings in wind farms.

The International Standardization Organization in its ISO16079–2:2020 standard states that multiple techniques exist for measuring high-frequency impacts by capturing stress waves generated from impacts between moving parts and surface imperfections. These techniques include ultrasound, shock pulse, acoustic emission, and stress wave analysis. Such methods are well suited for early detection of bearing failures, particularly in low-speed bearings [11]. As shown in Figure 2, which is regenerated depending on the standard ISO 16,079–2, there is a wide frequency range for detecting vibration-related failure modes on a WT. Our concern in this study is the first part of the range for detection of bearing faults, which spans between 4 Hz to about 100 Hz.

Even though detecting faults in low-speed bearings can be tricky to some extent, many studies have shown that AE is sensitive to low-speed bearing fault detection [5,12]. When compared with vibration, the received AE signal reflects the rapid release (transient) elastic waves caused by the sudden stress redistribution in solid material, which gives high sensitivity to detect early bearing defects [13]. This is the reason for adopting AE by many researchers to monitor the operating conditions of the low-speed bearing. In addition, Tang L. et al. proposed an algorithm based on time difference of arrival of AE signals for defect localisation detecting damage source localisation in large-size bearings [14].

M. Elforjani and Mba utilised AE signal to diagnose low-speed bearings and showed in more than one work [15–17] that AE energy can be reliable and sensitive for detecting incipient cracks in low-speed bearing. Additionally, Fuentes *et al.* [18] investigated the incipient damage in WT bearings. They used AE in practical sensing locations, and they constructed a probabilistic model to detect bearing sub-surface damage.

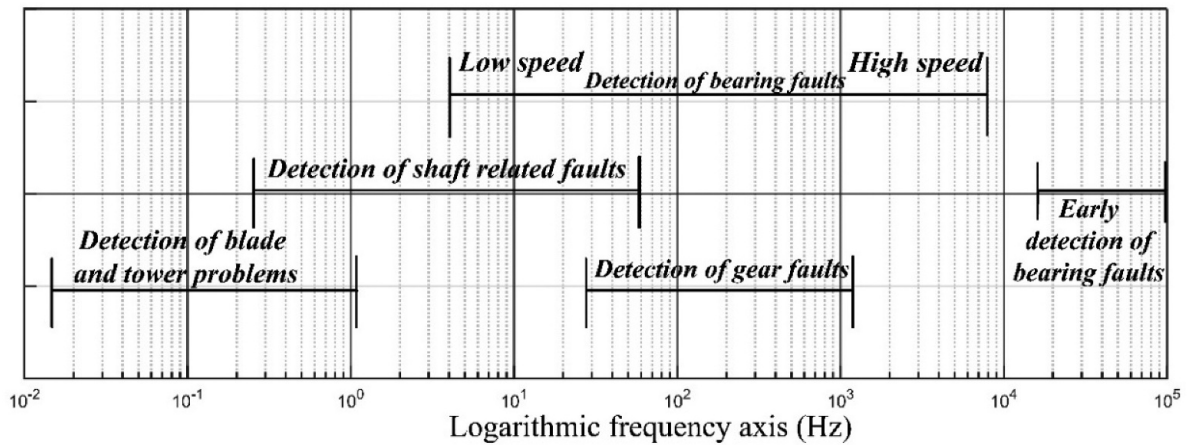


Figure 2. Typical representation of frequency ranges for failure modes on a WT [11].

The time domain analysis can be quite useful for low-speed applications, such as the low-speed shaft of the WT gearbox [19], the authors of the book confirm that AE has been proven able to detect faulty roller bearings at extremely low-speeds. They cited many studies that found AE parameters correlated with surface damage, such as pitting and scuffing, as well as with the generation and propagation of cracks.

While in the frequency domain, the dominant frequency (DF) of AE hits has been used in many studies recently as a parameter to investigate the micro-failure process of sandstones [20–22], rocks [23–26] (including granite [27] and marble [28,29]), asphalt [30], carbon/glass epoxy composites [31], and in welds [32]. However, to the best of our knowledge, DF has not yet been used in CM of machinery or energy assets, let alone in CM of bearings.

In summary, it can be concluded that, while vibration has traditionally been the predominant technique for monitoring rolling element bearings, particularly in WTs, the adoption of AE offers more comprehensive analyses of bearing condition and the potential to predict imminent defects before they appear in vibration signals. Recently, a trend to complement the AE analysis with vibration or other CM techniques has proved more inclusive and reliable, and it is becoming more popular among scholars [33].

While a substantial body of research exists on the use of AE for bearing analysis in general, its practical application on bearings in the field of wind energy remains limited to controlled laboratory environments under pre-defined conditions. This research gap highlights the need for implementation of AE-based CM of bearings in actual operating WT systems. By conducting field studies and collecting data directly from bearings in operational WTs, we can achieve a more accurate understanding of the practical limitations, advantages, and applicability of AE-based CM of bearings in WTs.

To address this research gap, our study aims to advance the practical application of AE in the context of wind energy by conducting measurements in real-world WT settings, utilising wireless techniques to establish an internet connection to a PC inside the nacelle, which is connected to an AE analysing system. This approach is cost-effective and easy-to-apply, and it provides access to real-time turbine data from anywhere on any device with internet.

The main objective of this study is to investigate the condition of the main shaft bearings in a 4-point suspension drivetrain configuration of a 2-Megawatt WT. This

configuration is characterised by having two bearings supporting the main shaft. We started a systematic analysis of the vibration signal that was received from one of the two monitored bearings and then applied a similar approach to the AE signal. The results from vibration analysis were validated and extended by the AE analysis.

More focus was put on the examination of AE signals in both time and frequency domains. AE parameters such as RMS and ASL were also used as a reference to give another perspective on the results. The analysis involved setting up a Post Processing Hit Detector (PPHD) to have the flexibility in specifying the parameters for detecting AE hits even in the offline mode. We transformed the AE signal using Fast Fourier Transform (FFT) to the frequency domain and then identified the DF of each AE hit that is detected by this PPHD. The DFs of the hits were then plotted on the time domain during specific time intervals to create the so-called DF map. While this technique has gained recognition in the field of geotechnical engineering, especially in recent years, it has not yet been adopted in mechanical applications, as shown in the literature review. We affirmed our findings and conclusions by overlaying many consecutive DF maps in one graph for each bearing to give a more comprehensive picture of the DFs for AE hits in each of the two bearings. The comparison between the two overlays of DF maps for the two monitored bearings gave the final judgement about the condition of the bearings. The use of DF maps showed distinct and well-defined frequency bands that enclosed groups of DFs of AE hits, which gives this method promising potential in the field of AE-based CM of bearings once the exact representation of these bands is established. This method is reliable and straightforward, which makes it possible to be automated and integrated in a predictive maintenance strategy.

The remaining sections of this paper are organised as follows: [Section 2](#) presents the measurement setup, the equipment, and the data acquisition procedure, [Section 3](#) describes and explains the vibration and AE analyses, in [Section 4](#) a discussion about the results is carried out, and [Section 5](#) presents the conclusions.

2. Methods and equipment

The measurements are taking place in a real-life environment on a WT of the type VESTAS 90/2.0 MW in South Moravia, the Czech Republic. This type of WTs with the 2-megawatt production is popular in that region, and it operates in a wind speed range between 4 and 25 m/s. The drivetrain of this WT is of the 4-point suspension type, which is characterised by a main shaft supported by two separate roller bearings. In the 4-point suspension drivetrain, the weight forces, the yawing and nodding moments from the rotor are transmitted to the nacelle's main frame, which means that the gearbox is protected against those effects.

The procedure of the measurement is shown in the schematic diagram in [Figure 3](#). Where two AE sensors and one vibration sensor were attached to the main shaft bearings. The sensors are connected to the AE analyser, which sends the converted signals to a PC for data acquisition and storage. The data is then transferred via the internet to our lab PCs for further analyses.

2.1. The application of AE as a CM technique

AE is a well-established Non-Destructive Testing (NDT) technique that allows the detection, monitoring, and localisation of defects in materials. AE is defined as the

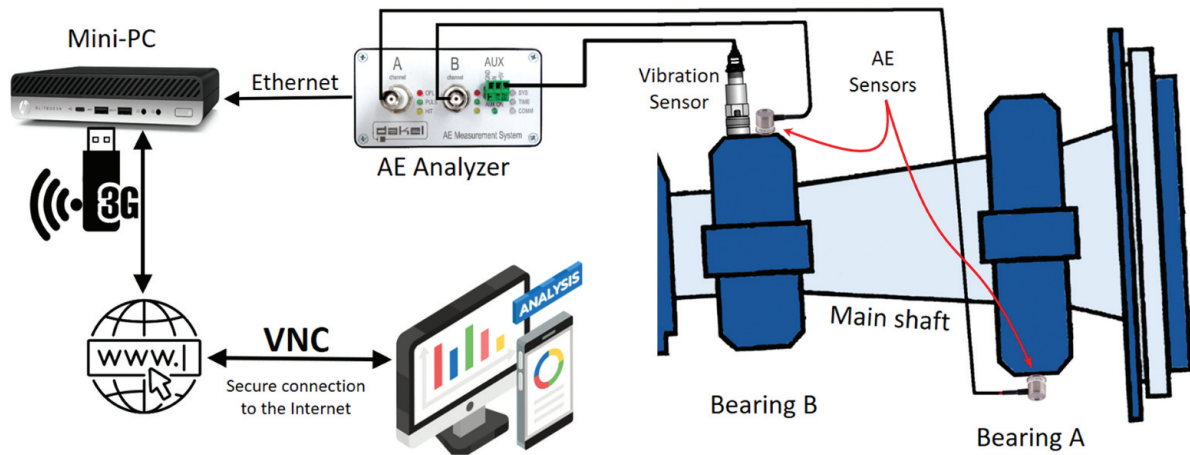


Figure 3. Schematic diagram of the measurement.

spontaneous release of localised strain energy in stressed material. This energy release can be due to micro-cracking in the material and can be recorded by transducers (sensors) attached to the material's surface [34]. The high sensitivity of AE measurements makes it susceptible to interference from the surrounding environment, but thanks to advances in measurement systems, the use of a bandpass filters effectively eliminates background noise and allows meaningful testing under normal conditions. The AE analyser (Zedo-Dakel) that we are using is equipped with two AE channels/cards and one auxiliary input channel that measures parametric voltage input (this channel was connected to the vibration accelerometer). [Figure 4](#) (Equipment) and [Figure 5 \(c\)](#) show the analyser fixed to the frame of the nacelle and connected to the mini-PC using an Ethernet cable. The analyser is also connected to the two AE sensors with coaxial cables. Each sensor contains an internal impedance converter and a preamplifier with a 35 dB gain. The sensitivity of the sensor is between 25 and 600 kHz. AE sensor that is connected to channel A is fixed firmly to the lowest point on the housing of bearing A, and AE sensor that is connected to channel B is fixed firmly to the top of the housing of bearing B, as shown in the schematic diagram in [Figure 3](#), [Figure 4](#), and in [Figure 5 \(a\)](#) and (b).

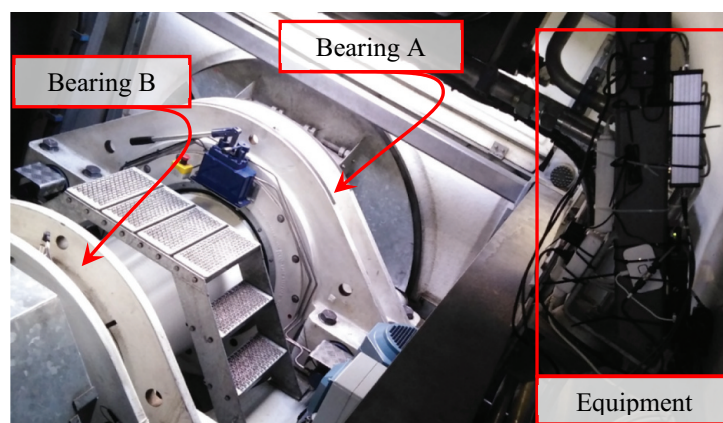


Figure 4. Position of the measuring equipment inside the nacelle.

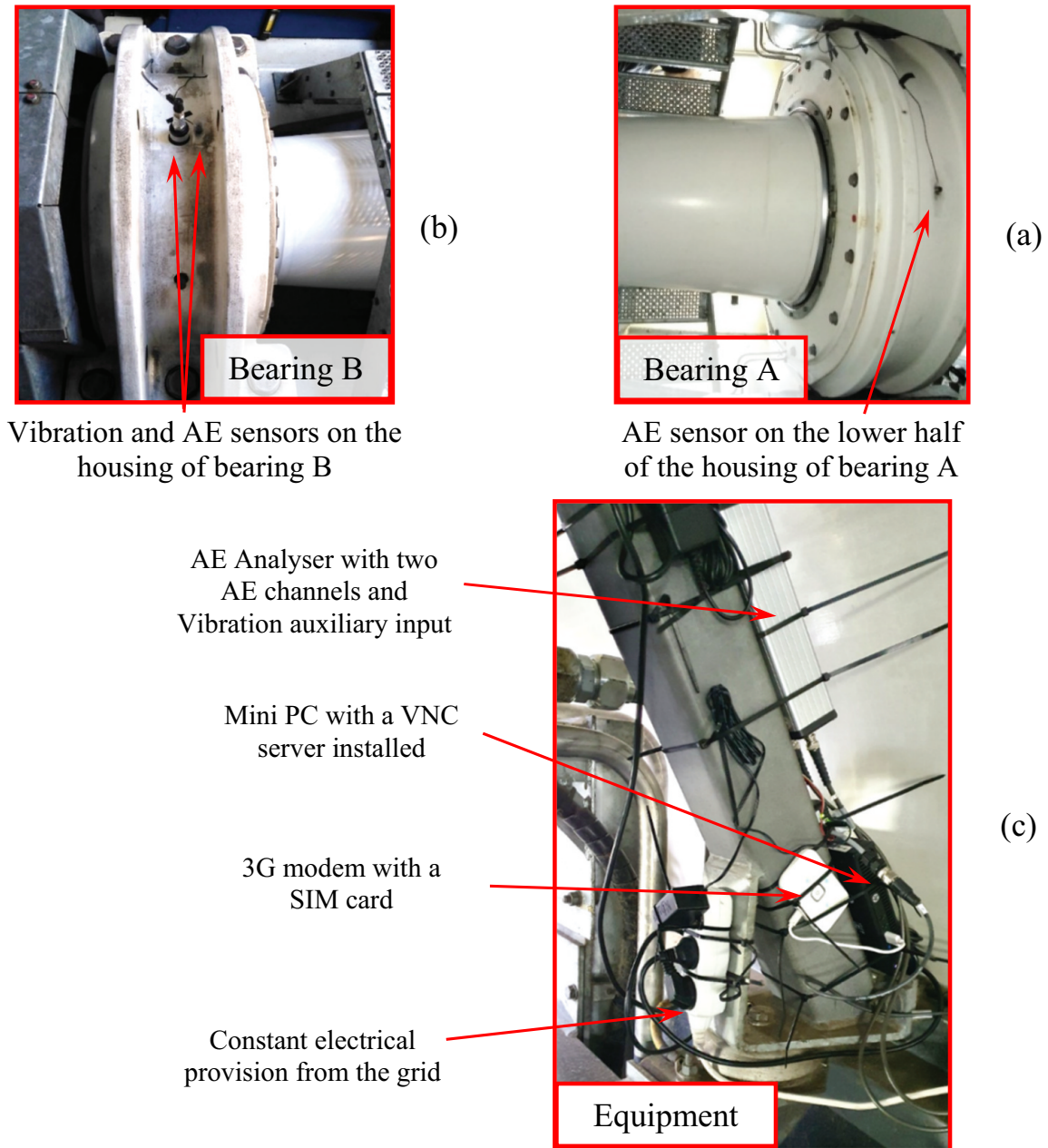


Figure 5. (a,b) Positions of AE sensors on the housings, (c) equipment for data acquisition, analysis and transmission from WT nacelle.

The sampling frequency for frequency spectrum computation is 2 MHz. The frequency bandwidth was limited by digital filters as follows: High-pass filter 20 kHz and Low-pass filter 500 kHz. The global measurement period for AE parameters was set to 1 s, which is a suitable compromise for long-term measurements. Some basic configurations on the AE analysis software included saving the full signal twice a day for a period of 30 s, and simultaneously recording the full vibration signal for those 30 s (twice a day, at 8:00:00 a.m. and at 04:00:00 p.m.).

As mentioned earlier, since our focus will be on the analysis of the frequency domain, we chose to use just two AE parameters, RMS and ASL. RMS is the most commonly used time-domain parameter of AE [35], and it is defined as:

$$AE_{RMS} = \sqrt{\frac{1}{\Delta T} \int_0^{\Delta t} V^2(t) dt} = \sqrt{\sum_{i=1}^N \frac{V^2(i)}{N}} \quad (1)$$

Where ΔT is the integration time constant, N is the number of discrete AE data within ΔT , and $V(i)$ is the voltage values of the signal from the sensor.

The average signal level (ASL) is another commonly used AE parameter, defined as:

$$ASL = \frac{1}{T} \int_{t_0}^{t_0+T} |v(t)| dt = \frac{1}{N} \sum_{n=1}^N |v(n)| \quad (2)$$

where t_0 is the initial time, T is the integration time of the signal and N is the number of discrete AE data within the interval T . $v(t)$ is the time-varying signal voltage.

Since we could not get information from the SCADA system of the WT, we applied our own real-time online monitoring system, by installing a mini PC (it has all the capabilities of a regular PC, but with compact design) connected to AE analyser inside the nacelle. They act as a local data acquisition unit, performing primary signal analysis and feature extraction processes. More demanding and advanced analyses are then performed on the extracted data after transmission via the internet to our laboratory computers.

To ensure seamless and secure data transmission, a 3G (third generation of digital mobile networks) internet connection was employed, by using a modem with a 3G SIM card connected to the PC, allowing continuous remote access to the mini PC within the WT's nacelle. Furthermore, a VNC (Virtual Network Computing) server software was installed (RealVNC®) to establish a secure and encrypted connection between the PC and any VNC viewer.

It is important here to distinguish between the case of wind farms and individual isolated WTs. The use of a highly sophisticated SCADA system in the case of wind farms consisting of a large number of WTs pays off on the long run. While in the case of individual stand-alone WTs, utilising a VNC server with a reliable 3G connection, the monitoring process becomes significantly streamlined and cost-effective. This approach eliminates the need for a complex and resource-intensive SCADA, and it allows direct access to real-time turbine data from anywhere, on any device that has access to the internet. Therefore, we are not suggesting this application as a replacement of SCADA, but as a complementary application to reduce complexity when possible.

The vibration transducer (accelerometer) that we used is from the type IEPE (Integrated Electronics Piezo-Electro); it has a built-in integrated circuit with a charge to voltage converter. The accelerometer is connected to Analogue-to-Digital Converter (ADC) in the auxiliary card of the AE analyser. It has a sensitivity value of 97.6 [mV/(m/s²)], and Bias = 11.5 [V]. The data that are received from the vibration transducer are raw acceleration. This signal is digitally processed and presented in the time domain, and then it is transformed to the frequency domain.

The sampling frequency of the vibration data is: $F_{s-v} = 1000$ Hz

The measurement procedure started in April 2022, and since then we have been monitoring and recording data about the condition of the main shaft bearings in the WT. Therefore, by the time of preparing this paper, we already have data for 1 year. We

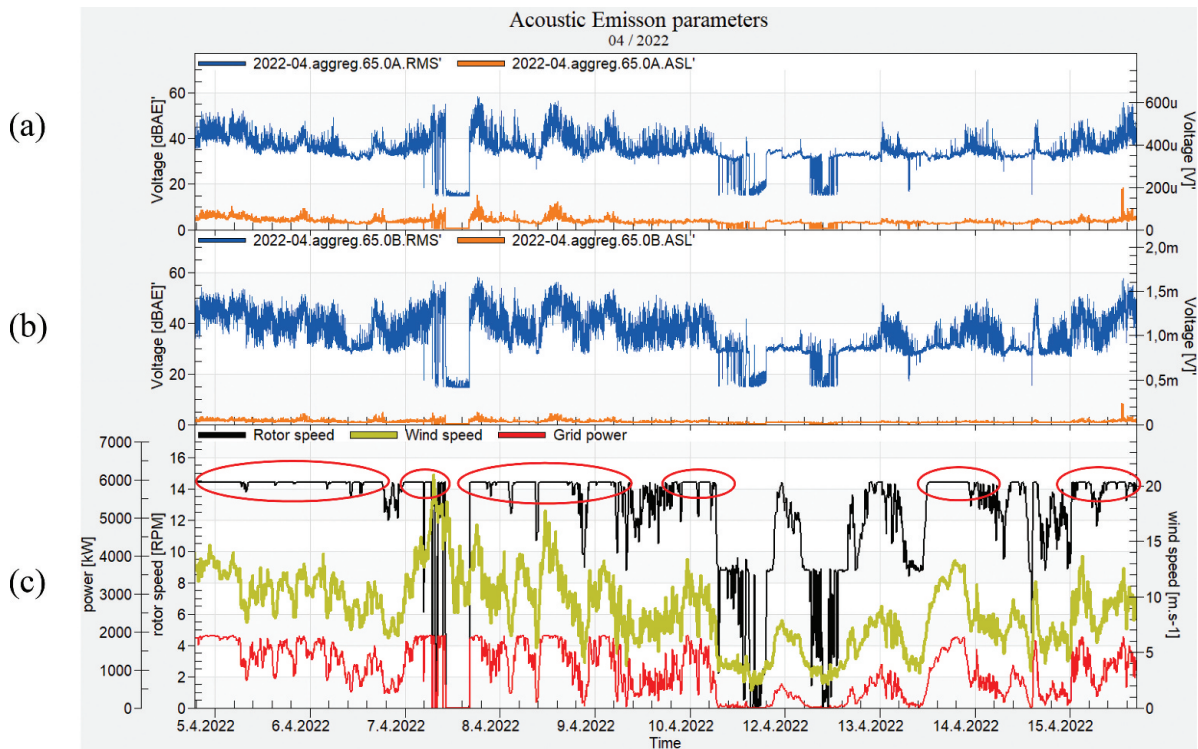


Figure 6. Operation data for the first two weeks in April 2022 (as an example). (a) RMS and ASL (aggregated) of AE from channel A. (b) RMS and ASL (aggregated) of AE from channel B. (c) WT operation parameters, rotor speed, wind speed, output power. Red ellipses are the places of the cut-out rotor speed, where data were picked to be analysed.

divided the recorded data into weeks, so for each week we have a block of data ready to be analysed separately.

Figure 6 shows the recorded data for 2 weeks in April 2022, as an example. It includes some of the most relevant operation parameters of the WT, such as the wind speed, rotor rotation speed, and the produced power to the grid in Figure 6(c), as well as some of the AE parameters such as RMS and ASL from both channels A and B, in Figure 6(a,b), which show that RMS and ASL are very responsive to the changes of rotor speed. This is more obvious in the periods of shutdown, for maintenance or for safety reasons, like the one that took place for a few hours on the middle of the day on 7th of April, where we see how this shutdown was clearly reflected in the signal. With this regard, it is worth mentioning that these results were in alignment with the findings of Luis, F. et al. [36], even though they did their study on the gearbox bearings.

We then sliced each block of data into segments where the full data were recorded, which means that twice a day, each time segment consists of 25 s of fully recorded AE and vibration data, we call them time slices. We concentrated on analysing the time slices where the rotation of the rotor was at its highest. Because as it is shown in Figure 6(c), marked by red ellipses, it is obvious that at these times the signal was the strongest, and the AE parameters were at their highest values.

This fixed highest speed for the rotor is considered as an advantage for monitoring the main shaft bearings in WT because it helps fix one of the main parameters, which is the rotation speed, for a period of time as long as the wind speed is above its cut-out value,

which is 25 (m/s). In our case, the cut-out rotation speed was set at 14.9 rpm. Therefore, we applied all the analyses on the signals just in these cut-out periods.

The duration of one cycle during the cut-out speed is $60/14.9 \approx 4$ s.

3. Results

3.1. Analysis of the vibration signal

The vibration signal was received from the accelerometer by ADC in the analyser, then to the software to be presented in the time domain, as shown in [Figure 7](#), the fully recorded time slice (25 s) of the vibration data. It contains many overlapped signals from different sources, and a lot of noise, which we cannot distinguish. Therefore, we transform it to the frequency domain. To do this we use Welch's method, which is a method based on time averaging over short, modified periodograms that uses FFT for the estimation of power spectra.

We chose the overlap between Welch windows to be 50% and the size of each window to be equal to the sampling rate, which is 1000 points.

To apply Welch's method and get the power spectrum of the signal, we extracted the data from the time domain and read it on MatLab®. The result is shown in [Figure 8](#). It shows the spectrum of frequencies of the signals that are combined in the vibration, and it distinguishes the frequencies that are dominant. We can tell from this figure that there are many signals received by the accelerometer with different frequencies, but the DF of vibration in this time interval is around 60 Hz.

The Y-axis in [Figure 8](#) is in logarithmic scale, so we remove this logarithmicity of Y, to get a more definitive curve for the DFs in the signal, as shown in [Figure 9](#).

We can see from [Figure 9](#) that the fundamental frequency of the vibration signal is around 60 Hz, and we can see the smaller peaks at its harmonics, the 120 Hz and 180 Hz. We can also see a peak at 0.25 Hz (=15 rpm), which is equal to the rotational speed of the main shaft. When comparing with the practical recommendations provided by [37–39], and with information from [Figure 2](#) (from ISO16079–2) which tells that a vibration frequency between [4–100] Hz indicates a bearing fault, we can assume with confidence that there are defects in bearing B. However, since the bearing is still in operation and the measurement is still running, we cannot carry out

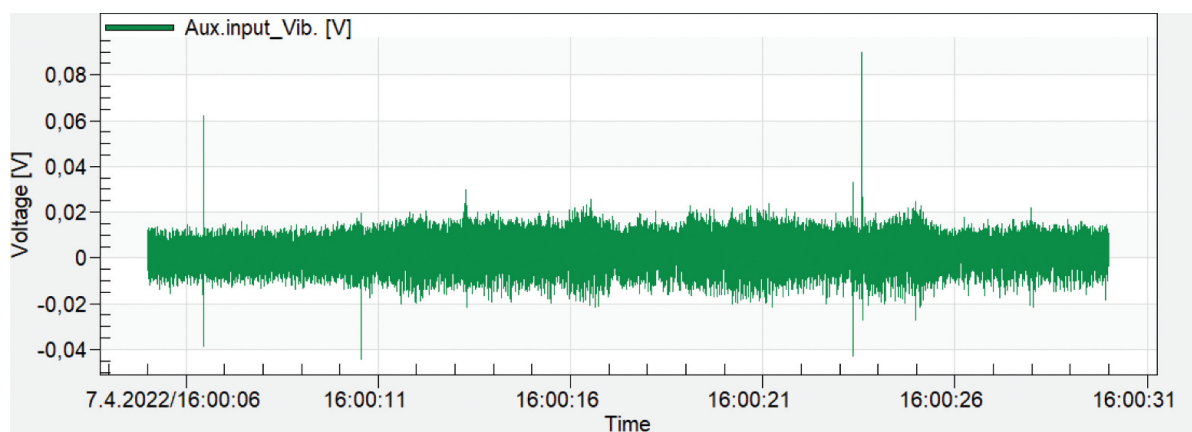


Figure 7. Fully recorded 25 seconds of vibration signal in the time domain.

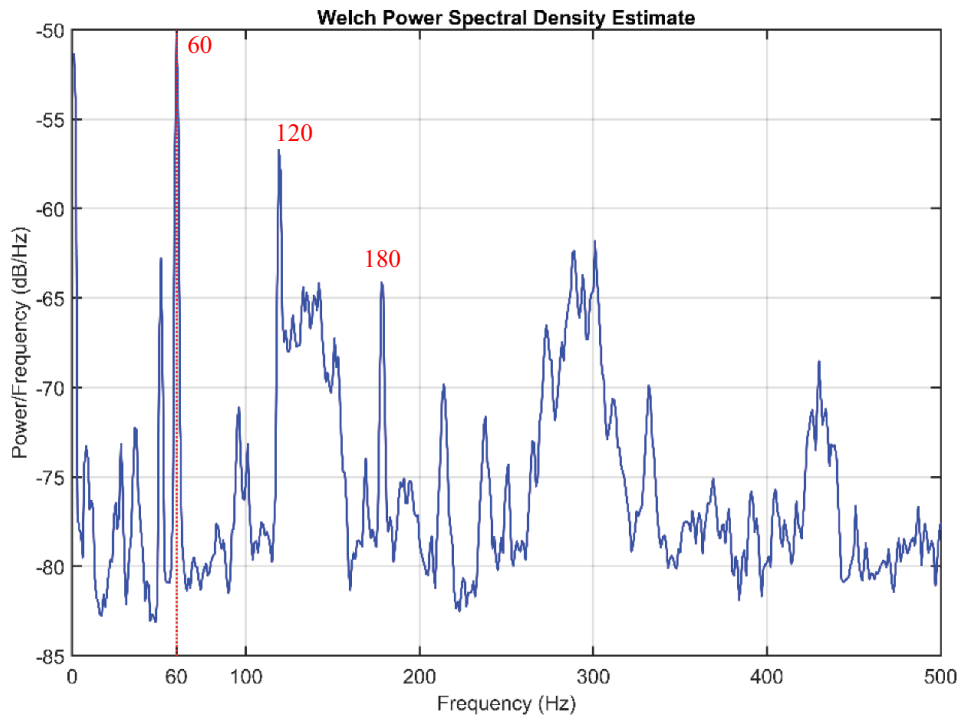


Figure 8. Power spectrum of the vibration signal using Welch estimate.

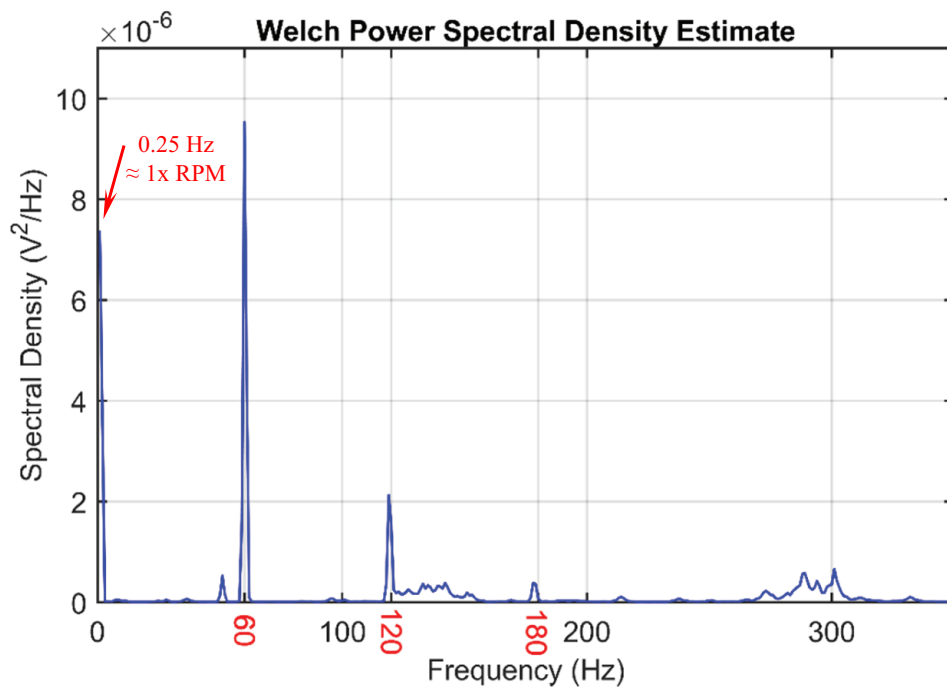


Figure 9. Spectrum after removing the logarithmicity of Y-axis.

physical inspections, which begs the need for extra investigation using different techniques; it is AE in our case.

3.2. Reading the vibration spectrogram

The spectrogram is a visual representation of the spectrum of frequencies in a signal over time, i.e. it is a time-frequency representation of the signal. Technically, it is the magnitude squared of the short-time Fourier transform (STFT) of the signal. The produced spectrogram in Figure 10(a) shows the changes of frequencies over time, while the intensity of the yellow colour represents the power of the signal.

Figure 10(b) is the same spectrum as in Figure 8 rotated by 90 degrees, which was achieved by applying Welch method for PSD estimation (Later in the AE analyses, we adopted the Welch method alone, because it gives a specific number for the dominant frequency in a 2D graph). To find which timestamps contain the highest spectral power, we sum the power across all frequencies for each timestamp. As shown in Figure 11, we summed all the spectral power values at each timestamp from the spectrogram (a) to make up the graph (b) in the time domain. Then we specify the maximum 10 values of the sum of signal's PSDs, or the 10 local maxima, as they are called in Figure 11(b). Then we superimpose those values back on the time domain, as shown in Figure 12.

When comparing Figures 12 with 7, we can see that some of the occurrences of the 10 maxima of PSD sums take place at the times where there is sudden increase in the vibration amplitude, and some do not, those are buried in the noise, but their timestamps were exposed by this method. In addition, we notice from the distribution of the maxima of PSD in Figure 12 and from other figures for other time slices that the occurrences have a kind of patterned appearance. The pattern might not look consistent in one figure (in 25-s slice), the consistency is related more to the distribution and the appearance of at least one maximum PSD value every 4 s. When taking into consideration the previous discussion on Figure 9, this patterned appearance of PSD maxima supports our previous assumption of existing defects on the bearing raceways.

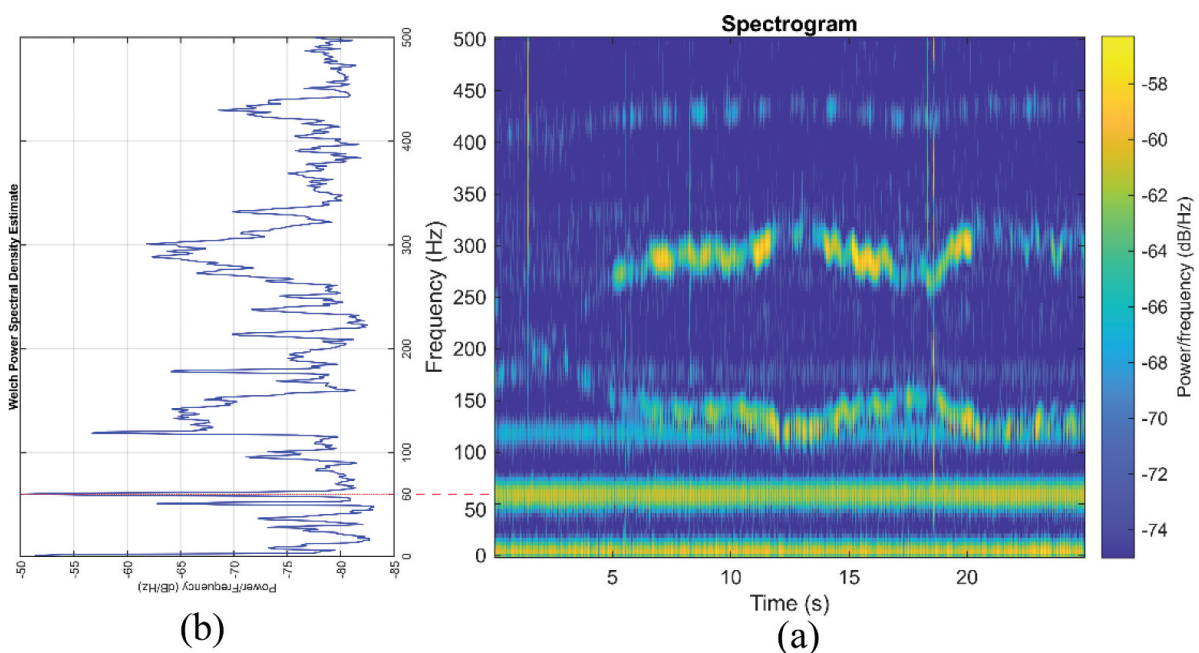


Figure 10. (a) Spectrogram of vibration signal, (b) with PSD of the signal.

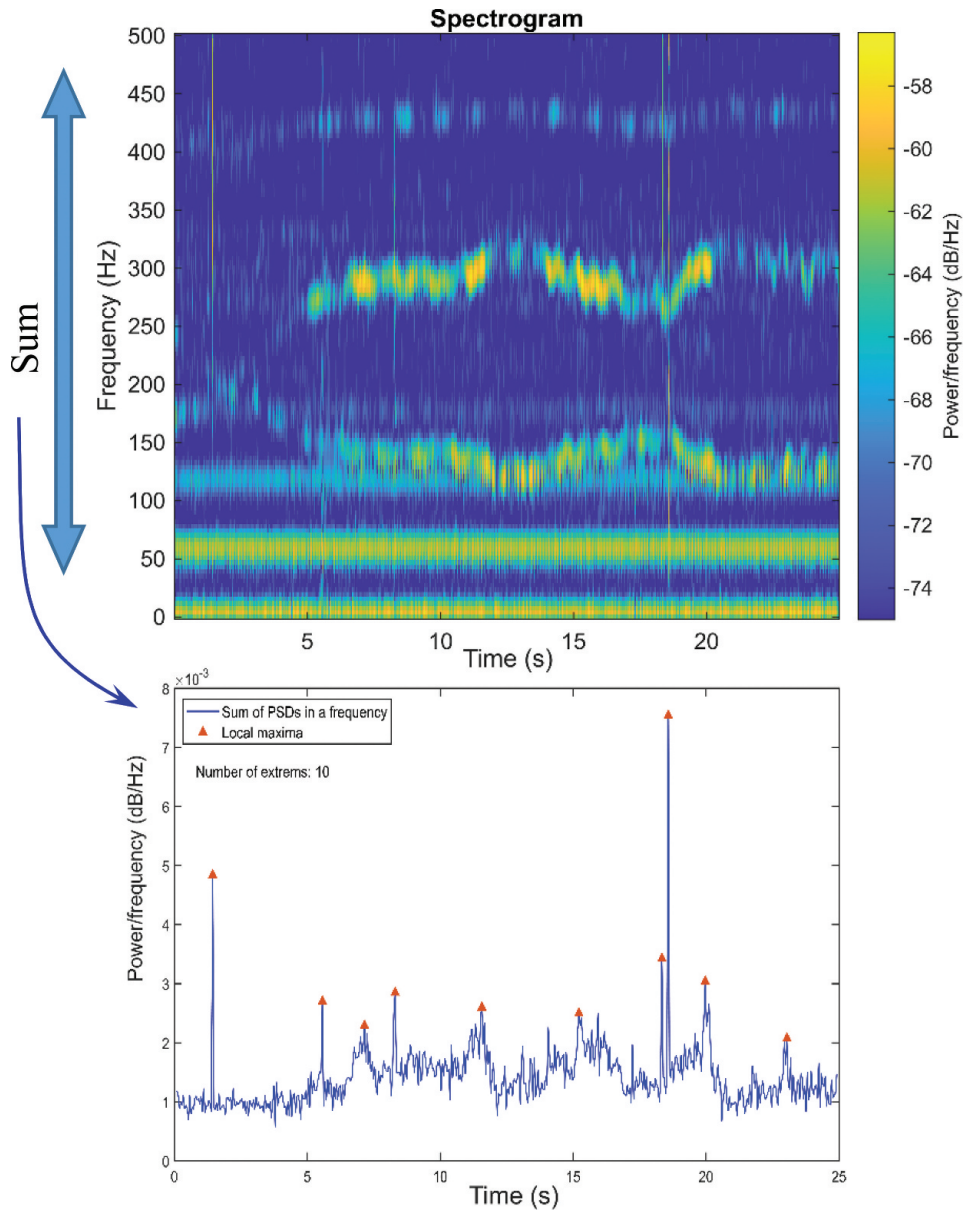


Figure 11. The spectrogram, with the sum of power densities extracted from it.

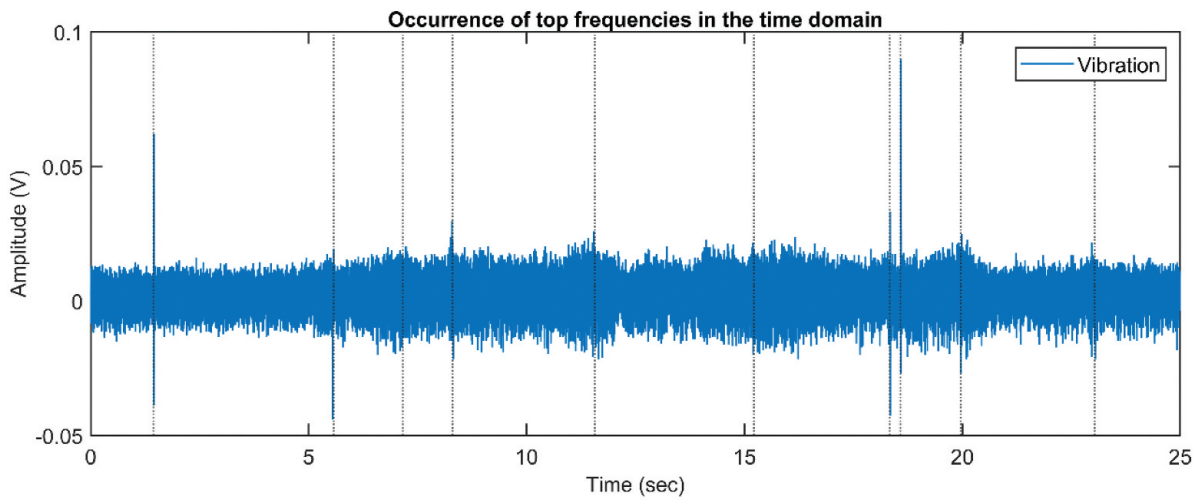


Figure 12. Superimposing the maximum 10 sums of PSDs on the time domain.

3.3. Analysis of AE signal

We applied similar sequence of actions for the analysis of the AE signal that was received from both sensors fixed to the bearings. Those steps are shown in the diagram in Figure 13. It consists of signal acquisition in the time domain, transforming the signal to the frequency domain using FFT, and identifying the DF for each AE hit in the time slice to create a DF map for all AE hits in that time slice. Many AE parameters were also extracted, but we chose to present just the RMS in correlation with the DFs in the time domain, since RMS is the mostly used AE parameter according to the literature, and because we are aiming at a signal-based analysis rather than a parameter-based one.

Figure 14 Shows one AE hit in the time domain that is detected by a PPHD. We established the PPHD to get more versatility in determining the parameters for the AE hit detector, even on the recorded signal (offline). The main setup parameters for the PPHD are given in Table 1.

The signal is then transformed to the frequency domain using FFT, to create the power spectrum shown in Figure 15. From this figure, the frequency corresponding to the highest power in the power spectrum is defined as the dominant frequency of the waveform signal. We can see from Figure 15 that DF for this AE sample is around 68 kHz.

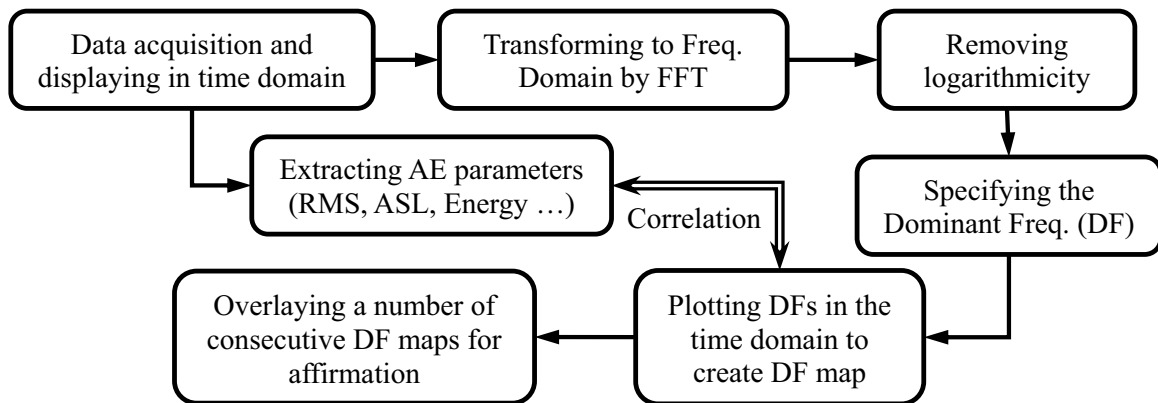
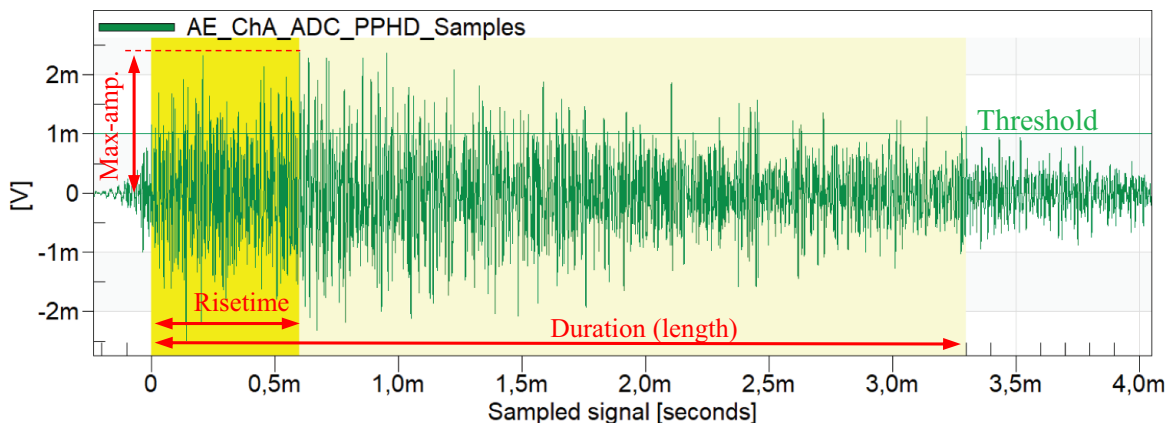


Figure 13. Sequence of steps for AE signal analysis.

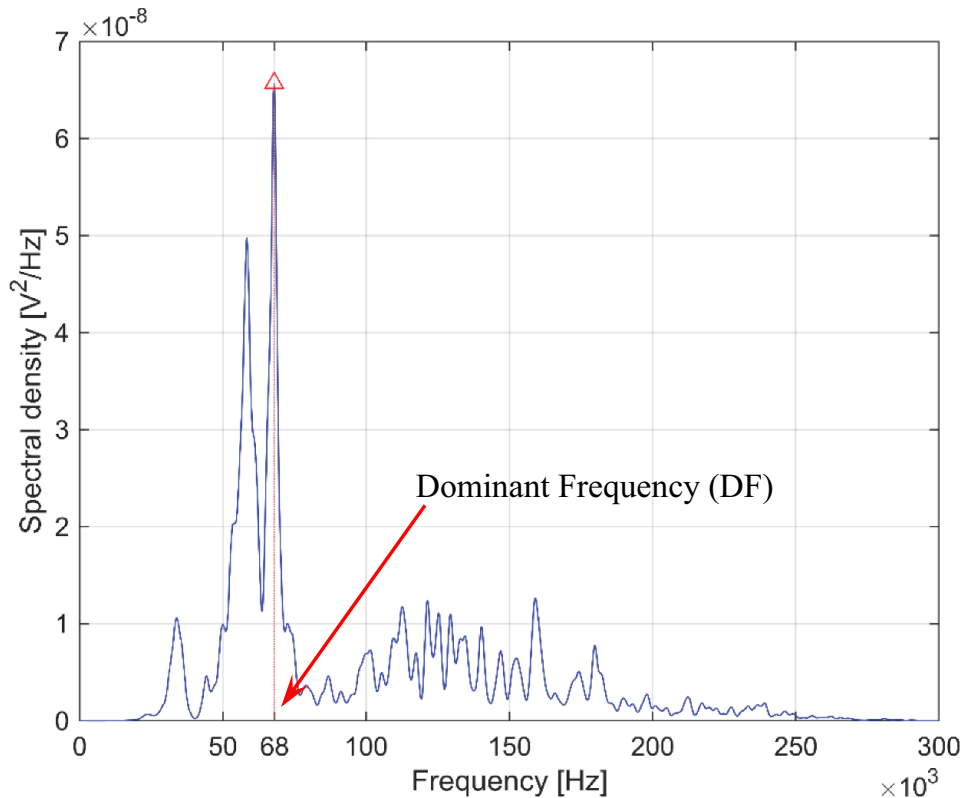


2022-04.aggreg.65.0A, Hit ID:21, Start:08:00:26.394_716_863, Length:3299.00 us, Risetime:600.5 us, Max-amp:67.5 dBAE (2.382 mV, 3.01%)

Figure 14. AE sample hit from channel a.

Table 1. The main setup parameters for the PPHD.

Parameter	Value
Detection threshold	1 mV (60 dBAE)
Separation time	1 ms
Dead time	10 ms
Minimum hit length	1 μ s
Maximum hit length	500 ms
FFT Calculation method	Welch estimate
Window size	8192
Window overlap	50%

**Figure 15.** Frequency domain of the AE hit shown in Figure 14.

We apply the same process to each AE hit detected by the PPHD. The DFs for all the detected hits in one time slice were then collected in one graph as shown in Figure 16(a,b) which are called the DF maps for bearing A and B, respectively. Figure 16 also shows the RMS of AE from both channels A and B.

Figure 16(a) shows that all DFs of the PPHD hits from bearing A fall inside two bands (ranges), the first band is [33–36] kHz which is a narrow band (enclosed inside a blue rectangle on the figure), and the second band spans from [60–77] kHz (enclosed inside a dashed red rectangle).

Figure 16(b) shows that all DFs of the PPHD hits from bearing B fall inside almost the same two bands: a narrow band [33–36] kHz (inside a blue rectangle) and another band [60–77] kHz (inside a dashed red rectangle).

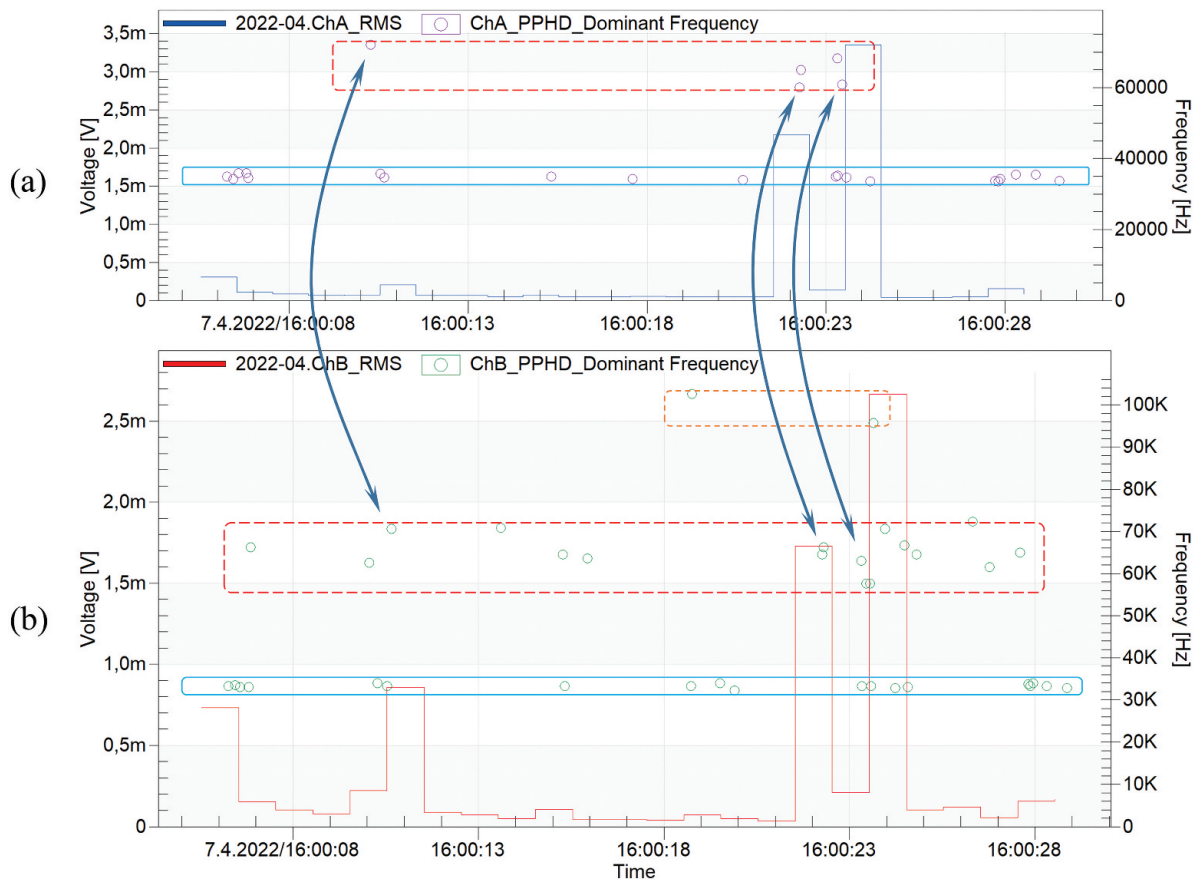


Figure 16. Frequency domain of the AE hit shown in Figure 14.

When comparing the two bands of DFs between the two bearings, we can see that the number of AE hits in the lower band is much bigger than the upper band and that most of the hits that have DFs in the lower frequency band [33–36] kHz are shared between the two bearings. They occur almost simultaneously or with minor shifts. However, by looking at the upper band of DFs [60–70] kHz, we can see that the number of hits differ greatly between the two bearings. Bearing B produces many more hits at these frequencies than bearing A. Bearing A produces hits at these frequencies just when RMS has an abrupt increase, and similar hits can be seen at these times from bearing B, as shown by the curved double-arrows on the figure.

On the other hand, when comparing the DFs of hits from both channels with the RMS from both channels in this time slice, we see some hits with similar DFs taking place even when the values of RMS are relatively low. This implies that RMS as an AE parameter does not capture or react to all the sources of the hits, so it cannot be depended upon solely for fully describing the condition of the monitored bearing.

Another intriguing aspect of the DFs from channel B is their patterned occurrence; they exhibit a patterned appearance where every 4–6 s there is at least one appearance of the maximum PSD. When taking into consideration the rotational speed of the shaft, which is about 4 s for one full rotation at the time of measurement, and considering the inevitable sliding effect of the rollers, we can assume that those DFs belong to hits that are

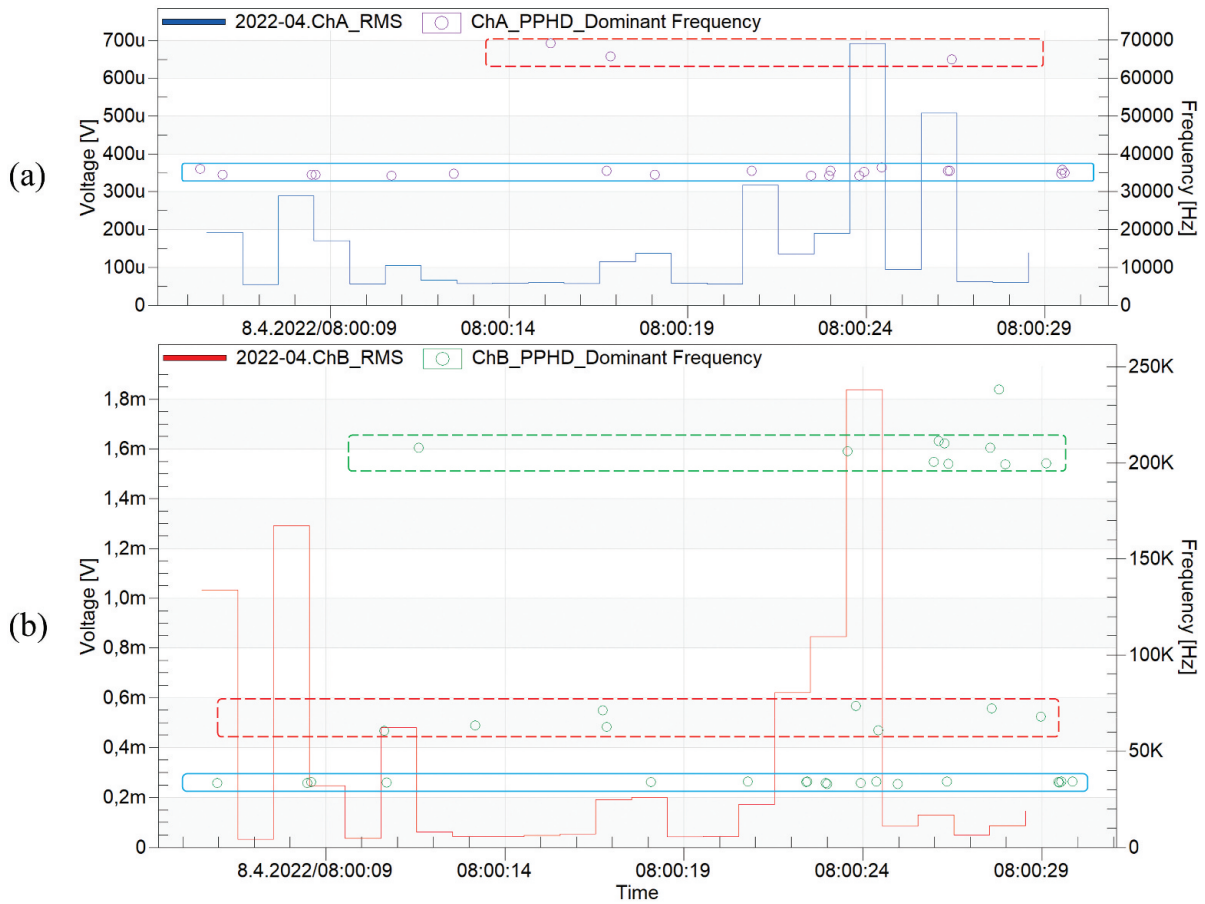


Figure 17. DF map for bearings a and B. (a) DFs of the PPHD hits from bearing A, (b) DFs of the PPHD hits from bearing B.

related to the rotation speed of the inner ring, and they are results of defects on the raceways.

We also see in [Figure 16\(b\)](#) a number of hits which were received just from channel B, whose DFs are in a band between [95–105] kHz (enclosed inside a dashed orange rectangle). They have no counterpart from channel A on [Figure 16\(a\)](#) or on any other DF map. [Figure 17\(a,b\)](#) is just another example of DF maps for bearings A and B, respectively, taken in different time slices. [Figure 17\(b\)](#) shows a group of hits with even higher DFs that range between [195–215] kHz (enclosed in a green rectangle). From [figure 16\(b\) and 17\(b\)](#) we can tell that those groups of hits that have the highest DFs are not correlated strictly to the RMS values.

3.4. Combining a number of subsequent DF maps

The preceding findings were observed in many other analysed time slices. Therefore, we produced the DF maps for a number of consecutive time slices in consecutive days and combined (overlaid) them in one graph for each bearing, as shown in [Figures 18 and 19](#) for bearings A and B, respectively (Note: The samples of DF maps are not distributed regularly on the time axis, because the chosen time slices, where the rotation speed was fixed at its maximum, were not regularly distributed).

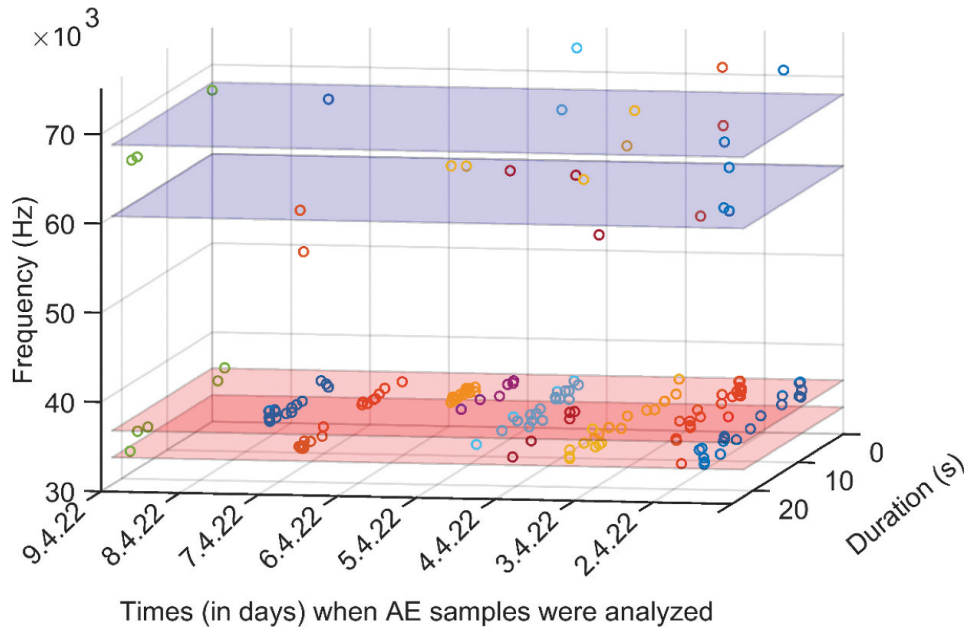


Figure 18. The overlay of some consecutive DF maps for bearing A.

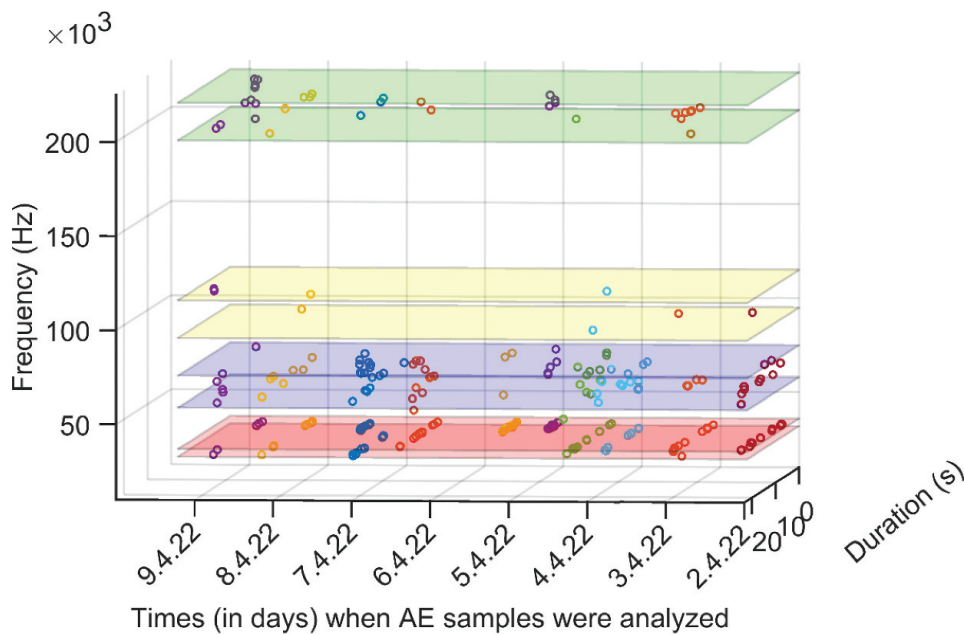


Figure 19. The overlay of some consecutive DF maps for bearing B.

The overlay of DF maps for bearing B in [Figure 19](#) confirms the existence of the two bands of high DFs, [95–105] kHz and [195–215] kHz, on some consecutive DF maps. Those two high DF bands do not appear in any of the DF maps of bearing A.

4. Discussion

Our objective to advance the AE-based CM of the main shaft bearings in WTs led us to employ the DF of AE hits as a parameter to indicate the condition of the bearings. For this purpose, we produced DF maps for each bearing in different time

intervals, and then we overlaid many consecutive DF maps for each bearing in one graph to affirm the consistency of the results and to give a better overview of the condition of the bearing. In our case study, the comparison between the two overlays of DF maps over the same period gave a confirmation of the preceding vibration analysis that was carried out on bearing B, which indicated the existence of defects on the bearing raceways, and showed that it is in a worse condition than bearing A.

When comparing the two overlays of DF maps for the two bearings in [Figures 18 and 19](#), we see that the two high DF bands, [95–105] and [195–215] kHz, appear only in DF maps for bearing B and do not exist in DF maps for bearing A.

Combining this observation with the conclusion that we reached after the vibration analysis of bearing B (after [Figure 12](#)) gives more support to the presumption of the existence of defects on the raceways of bearing B. It also indicates that those defects are of different types and sizes.

Another observation is that the number of AE hits in the middle DF band [60–77] kHz for bearing B is bigger than the number of AE hits for bearing A in that frequency band. Those hits show patterned appearance, where each 4 s we see at least one hit. We suspect that this band of DFs is the most indicative of defects on the bearing raceways.

We also notice that both bearings have the highest number of AE hits in the lowest DF band [33–36] kHz, and we can indicate from the number of those hits and their distribution, that most of them are attributed to noise and external sources.

One of the frequent observations was also that the RMS, when compared to the occurrence of AE hits on DF maps, did not capture all the events, as seen in [Figures 16 and 17](#) and the discussion on them. Even though a substantial amount of research on AE-based CM of bearing considered AE parameters as credible indications of defects in bearings [5,16,18,36,40] to name a few. Our observations do not contradict with that, as seen in [Figure 6](#), and as we stated when comparing our results to the model developed by Luis, F. et al. [36]. AE parameters are credible indications of defects, but adding DF of AE hits as a parameter will increase their credibility.

One fact that we should address is that the boundaries of DF bands are not strictly defined. We see from the overlays that there are some scattered hits, which have DF outside the defined DF bands, but they are non-repetitive, they appear randomly, so they are unlikely to be the result of defects in the cyclically rotating elements of the bearing.

Since the comparison between the two bearings was a key factor in the conclusion, we acknowledged that this approach is applicable only to the type of WTs that have two bearings supporting the main shaft, as in the 4-point suspension drivetrain. However, with the existence of enough historical data from similar configurations, this limitation could be mitigated. Another drawback is that the comparison leads to a relative conclusion. Therefore, even though it confirmed that bearing B is in a worse condition than bearing A, it did not give an accurate description of the condition of bearing A, as long as the exact interpretation of the DF bands has not been known yet. In addition, we believe that utilising DF of AE hits in bearings CM research will contribute to establishing a reliable database that can be used to determine the possible causes of AE hits within each DF band. Another factor that contributed to this drawback (specifying the condition of bearing A) is the fact that we used only one vibration transducer attached to bearing B; this was due to the analyser being equipped with only one auxiliary card for the extra

parameter analysis. We will solve this limitation with the manufacturer for the upcoming measurements.

With regard to CM of bearings, combining the traditional vibration analysis with AE analysis has been popular in research, with concentration on the parameter-based analysis of the AE, applying many new techniques on the AE-extracted parameters. However, to the best of our knowledge, the DF of AE hits has not been explored yet as an indicator for CM of machinery or mechanical components, let alone of bearings, even though this technique has been gaining a lot of attention in fields like Geotechnical engineering, as shown in the literature review. To the extent that we find the statistical characteristics of DF of AE hits being examined in prior works [28,29], then these statistics have been utilised, depended upon, and extended in subsequent studies [21–23,25–27]. The only exception we were able to find was the work of Haneef et al. [32] when they used frequency centroid in their study on steel welds and they mentioned the DF of AE, but they did not use it the way we did in this work. Therefore, we can claim to be the first who used the DF of AE hits on bearings, accompanied by vibration analysis, and we intend to continue to use this technique in our future investigations.

In our work, unlike the studies that used the DF of AE hits, we added an extra step of affirming the consistency of our findings by overlaying many consecutive DF maps on one graph for each bearing to give a more comprehensive picture of the DFs for AE hits in each of the two bearings.

We also created a batch-processing programme for this function to simplify our current work, and to make it a basis for the planned future advancement of the automation of this process. Our future steps also include extending the application of our CM system to other WTs with varying service lifespans, which will enable us to conduct a comparative analysis of the results. We also have to improve our current signal processing procedure accordingly, which will help us develop advanced predictive maintenance strategies for different WTs.

Finally, we would like to initiate a call for further exploration and interest in the employment of DF of AE hits as a valuable parameter for AE-based CM of bearings, as it has shown promise and success in other fields. Its novel implementation in the realm of bearing CM requires more research and validation through collaborative efforts and interdisciplinary investigations.

5. Conclusion

In this work, we investigated the structural health of the two main shaft bearings in a 4-point suspension drivetrain configuration of a 2-Megawatt WT. Our investigation focused on examining and analysing AE signals emanating from both bearings in the time and frequency domains. Vibration analysis was also applied to one of the bearings and it led to the presumption that the smaller bearing B has developed defects on the raceways. The analysis of the AE signal confirmed this and showed that those defects are of different types and sizes. It demonstrated that bearing B is in a worse condition than the bigger bearing A.

Our analysis on the frequency domain of AE hits led to the creation of DF maps for each bearing. The DF map is a representation in the time domain of the DFs of all AE hits received from the PPHD in specific time intervals. Overlaying many DF maps over many consecutive intervals gave more confirmation of the

results and a more comprehensive view of the condition of the bearings. To the best of our knowledge, the principle of DF maps has not been used in the field of CM of bearings, and we believe it has promising potential in this field as a method for representing the condition of a bearing. It was apparent from the DF maps that the DFs of AE hits are grouped in well-defined bands. Those groups presumably represent different types and sizes of defects. The exact correlation between the sizes of the defects and the DFs requires further investigation. An important observation was that AE parameters, such as RMS, did not completely correspond to the events that were represented by the occurrence of AE hits, which leads to the conclusion that AE parameters alone cannot be depended upon for the determination of the condition of a bearing. The comparison between DF maps for both bearings, taken simultaneously, provided the basis for assessing the condition of the bearings. Implying that it is suitable only for drivetrain arrangements that is characterised by two bearings supporting the main shaft (which is the preferable drivetrain arrangement in big multi megawatt WTs). One of the advantages of this method is the simplicity, where all the Matlab® codes can be combined, automated and integrated into a CM system for the drivetrain of WTs and then for the development of a predictive maintenance strategy to mitigate the potential risks of such invaluable assets.

We also introduced an easy-to-apply method for continuous online monitoring of the main shaft bearings that is particularly useful in the case of stand-alone WTs. The method utilises a 3G connection and a VNC server. We have been using it reliably for more than a year for monitoring and recording data.

Acknowledgments

This research was supported by the National Competence Centre of Mechatronics and Smart Technologies for Mechanical Engineering under the project TN02000010. It is co-financed by the Technology Agency of the Czech Republic (TACR). The authors would also like to thank Dakel-Center of Technical Diagnostics, the AE Company that provided all the equipment.

Disclosure statement

The authors declare that they have no known competing financial interests or personal relationships that could have appeared to influence the work reported in this paper.




Funding

This work was supported by the National Competence Centre of Mechatronics and Smart Technologies - The Czech Republic [TN02000010]; National Competence Centre of Mechatronics and Smart Technologies [TN02000010].

ORCID

Housam Mohammad  <http://orcid.org/0000-0003-2955-7112>

Frantisek Vlasic  <http://orcid.org/0000-0002-5283-2461>

Jiri Zacek  <http://orcid.org/0000-0002-2883-6702>
Baraah Maya  <http://orcid.org/0000-0002-9868-2358>
Pavel Mazal  <http://orcid.org/0000-0003-1766-4666>

References

- [1] LEE J, ZHAO F, et al. 2022. GWEC | GLOBAL WIND REPORT. Brussels, Belgium: Global Wind Energy Council; p. 155. Available at: https://gwec.net/wp-content/uploads/2022/04/Annual-Wind-Report-2022_screen_final_April.pdf
- [2] DAO C, KAZEMTABRIZI B, CRABTREE C. Wind turbine reliability data review and impacts on levelised cost of energy. *Wind Energy*. 2019;22(12):1848–1871. ISSN 1095-4244. doi: [10.1002/we.2404](https://doi.org/10.1002/we.2404)
- [3] FAULSTICH S, HAHN B, TAVNER PJ. Wind turbine downtime and its importance for offshore deployment. *Wind Energy*. 2011;14(3):327–337. ISSN 10954244. doi: [10.1002/we.421](https://doi.org/10.1002/we.421)
- [4] AZEVEDO DE, Dias Machado H, Araújo AM, et al. A review of wind turbine bearing condition monitoring: state of the art and challenges. *Renew Sust Energ Rev*. 2016;56:368–379. doi: [10.1016/j.rser.2015.11.032](https://doi.org/10.1016/j.rser.2015.11.032). ISSN 13640321.
- [5] CAESARENDRA W, KOSASIH B, TIEU AK, et al. Acoustic emission-based condition monitoring methods: review and application for low speed slew bearing. *Mech Syst Signal Process*. 2016;72-73:134–159. ISSN 08883270. doi: [10.1016/j.ymssp.2015.10.020](https://doi.org/10.1016/j.ymssp.2015.10.020).
- [6] CAESARENDRA W, KOSASIH B, TIEU AK, et al. Application of the largest Lyapunov exponent algorithm for feature extraction in low speed slew bearing condition monitoring. *Mech Syst Signal Process*. 2015;50-51:116–138. ISSN 08883270. doi: [10.1016/j.ymssp.2014.05.021](https://doi.org/10.1016/j.ymssp.2014.05.021).
- [7] LIU ZALZ, Zhang L. A review of failure modes, condition monitoring and fault diagnosis methods for large-scale wind turbine bearings. *Measurement*. 2020;149:149. ISSN 02632241. doi: [10.1016/j.measurement.2019.107002](https://doi.org/10.1016/j.measurement.2019.107002).
- [8] GBASHI S, Nkosinathi MADUSHELE M, Obafemi OO, et al. Wind turbine main bearing: a mini review of its failure modes and condition monitoring techniques. In: 2022 IEEE 13th International Conference on Mechanical and Intelligent Manufacturing Technologies (ICMIMT). IEEE, 2022, s. 127–134. ISBN 978-1-6654-8400-8: doi:[10.1109/ICMIMT55556.2022.9845317](https://doi.org/10.1109/ICMIMT55556.2022.9845317)
- [9] JIN S, DONG H, CHEN J, et al. Study on accelerated life tests for main shaft bearings in wind turbines. *J Mech Sci Technol*. 2022;36(3):1197–1207. ISSN 1738-494X. doi: [10.1007/s12206-022-0116-8](https://doi.org/10.1007/s12206-022-0116-8)
- [10] Zhipeng MA, ZHAO M, Mourui LUO, et al. An integrated monitoring scheme for wind turbine main bearing using acoustic emission. *Signal Process*. 2023;205:108867. doi: [10.1016/j.sigpro.2022.108867](https://doi.org/10.1016/j.sigpro.2022.108867).
- [11] Condition monitoring and diagnostics of wind turbines — part 2: monitoring the drivetrain. First. Switzerland: ISO: 2020. Technical Committee ISO/TC 108 - SC 5
- [12] VAN HECKE B, YOON J, David HE. Low speed bearing fault diagnosis using acoustic emission sensors. *Appl Acoust*. 2016;105:35–44. ISSN 0003682X. doi: [10.1016/j.apacoust.2015.10.028](https://doi.org/10.1016/j.apacoust.2015.10.028).
- [13] WANG Z, WU X, LIU X, et al. Research on feature extraction algorithm of rolling bearing fatigue evolution stage based on acoustic emission. *Mech Syst Signal Process*. 2018;113:271–284. ISSN 08883270. doi: [10.1016/j.ymssp.2017.08.001](https://doi.org/10.1016/j.ymssp.2017.08.001).
- [14] TANG L, LIU X, WU X, et al. Defect localization on rolling element bearing stationary outer race with acoustic emission technology. *Appl Acoust* 2021;182. ISSN 0003682X [10.1016/j.apacoust.2021.108207](https://doi.org/10.1016/j.apacoust.2021.108207).
- [15] ELFORJANI MADM, Mba D. Assessment of natural crack initiation and its propagation in slow speed bearings. *Case Stud NondestrTest Eval*. 2009;24(3):261–275. ISSN 1058-9759. doi: [10.1080/10589750802339687](https://doi.org/10.1080/10589750802339687)

- [16] ELFORJANI M, MBA D, CHARNLEY B. Observations of a naturally degrading slow-speed shaft. *Case Stud NondestrTest Eval.* 2010;25(4):267–278. ISSN 1058-9759. doi: [10.1080/10589750903473625](https://doi.org/10.1080/10589750903473625)
- [17] ELFORJANI MADM, Mba D. Accelerated natural fault diagnosis in slow speed bearings with acoustic emission. *Eng Fract Mech.* 2010;77(1):112–127. ISSN 00137944. doi: [10.1016/j.engfracmech.2009.09.016](https://doi.org/10.1016/j.engfracmech.2009.09.016)
- [18] FUENTES R, DWYER-JOYCE RS, MARSHALL MB, et al. Detection of sub-surface damage in wind turbine bearings using acoustic emissions and probabilistic modelling. *Renewable Energy.* 2020;147:776–797. ISSN 09601481. doi: [10.1016/j.renene.2019.08.019](https://doi.org/10.1016/j.renene.2019.08.019).
- [19] JANTARA VL, PAPAELIAS M. Wind turbine gearboxes: failures, surface treatments and condition monitoring. In: *Non-destructive testing and Condition Monitoring Techniques for Renewable Energy Industrial assets.* Elsevier; 2020pp. s. 69–90 ISBN 9780081010945. doi: [10.1016/B978-0-08-101094-5.00005-8](https://doi.org/10.1016/B978-0-08-101094-5.00005-8)
- [20] ZHANG H, LU K, ZHANG W, et al. A comprehensive study of damage characteristics and acoustic emission response mechanism of sandstone with different water contents. *Eng Fract Mech.* 2023;288. ISSN 00137944. doi: [10.1016/j.engfracmech.2023.109392](https://doi.org/10.1016/j.engfracmech.2023.109392).
- [21] LEI R, ZHANG Z, BERTO F, et al. Cracking process and acoustic emission characteristics of sandstone with two parallel filled-flaws under biaxial compression. *Eng Fract Mech.* 2020;237. ISSN 00137944. doi: [10.1016/j.engfracmech.2020.107253](https://doi.org/10.1016/j.engfracmech.2020.107253).
- [22] NIU Y, ZHOU X-P, BERTO F. Temporal dominant frequency evolution characteristics during the fracture process of flawed red sandstone. *Theor Appl Fract Mech.* 2020;110. ISSN 01678442. doi: [10.1016/j.tafmec.2020.102838](https://doi.org/10.1016/j.tafmec.2020.102838).
- [23] ZHU J, DENG J, PAK RYS, et al. Experimental study on the failure process of water-bearing rock under uniaxial tension based on dominant frequency analysis of acoustic emission. *Bull Eng Geol Environ.* 2023;82(6). ISSN 1435-9529. doi: [10.1007/s10064-023-03246-9](https://doi.org/10.1007/s10064-023-03246-9)
- [24] WANG C, CAO C, LIU Y, et al. Experimental investigation on synergetic prediction of rockburst using the dominant-frequency entropy of acoustic emission. *Nat Hazards.* 2021;108(3):3253–3270. ISSN 0921-030X. doi: [10.1007/s11069-021-04822-6](https://doi.org/10.1007/s11069-021-04822-6)
- [25] ZHU J, DENG J, CHEN F, et al. Water-weakening effects on the strength of hard rocks at different loading rates: an experimental study. *Rock Mech Rock Eng.* 2021;54(8):4347–4353. ISSN 0723-2632. doi: [10.1007/s00603-021-02482-3](https://doi.org/10.1007/s00603-021-02482-3)
- [26] ZHANG ZHAJHD, Deng J-H. A new method for determining the crack classification criterion in acoustic emission parameter analysis. *Int J Rock Mech Min Sci.* 2020;130:130. ISSN 13651609. doi: [10.1016/j.ijrmms.2020.104323](https://doi.org/10.1016/j.ijrmms.2020.104323).
- [27] WANG T, WANG L, XUE F, et al. Identification of crack development in granite under triaxial compression based on the acoustic emission signal. *Int J Distrib Sens Netw.* 2021;17(1). ISSN 1550-1477. doi: [10.1177/1550147720986116](https://doi.org/10.1177/1550147720986116)
- [28] ZHANG Z-H, DENG J-H, A Lin-Rui LI J-BZ. An experimental investigation of the failure mechanisms of jointed and intact marble under compression based on Quantitative analysis of acoustic emission Waveforms. *ROCK MECH ROCK ENG.* 2018;51(7):2299–2307. ISSN 0723-2632. doi: [10.1007/s00603-018-1484-3](https://doi.org/10.1007/s00603-018-1484-3)
- [29] LI LR, DENG JH, ZHENG L, et al. Dominant frequency characteristics of acoustic emissions in white marble during direct tensile tests. *Rock Mech Rock Eng.* 2017;50(5):1337–1346. ISSN 0723-2632 doi: [10.1007/s00603-016-1162-2](https://doi.org/10.1007/s00603-016-1162-2)
- [30] XU J, LUO X, QIU X, et al. Wavelet and fractal analysis of acoustic emission characteristic of fatigue damage of asphalt mixtures. *Constr Build Mater* 2022;349. ISSN 09500618. doi: [10.1016/j.conbuildmat.2022.128643](https://doi.org/10.1016/j.conbuildmat.2022.128643).
- [31] WOO SANG, GOO N. Analysis of the bending fracture process for piezoelectric composite actuators using dominant frequency bands by acoustic emission. *Compos Sci Technol.* 2007;67(7–8):1499–1508. ISSN 02663538. doi: [10.1016/j.compscitech.2006.07.023](https://doi.org/10.1016/j.compscitech.2006.07.023)
- [32] HANEEF TK, CHAKRABORTY G, REJEESH R, et al. Characterisation of hydrogen assisted cracking in modified 9Cr-1Mo steel welds using acoustic emission non destructive technique. *Case Stud NondestrTest Eval.* 2021;36(6):692–708. ISSN 1058-9759. doi: [10.1080/10589759.2021.1889547](https://doi.org/10.1080/10589759.2021.1889547)

- [33] DENG L, LIU S, SHI W, et al. Defect detection and classification of offshore wind turbine rotor blades. *Case Stud NondestrTest Eval.* 2023;1–22. ISSN 1058-9759. doi:[10.1080/10589759.2023.2234554](https://doi.org/10.1080/10589759.2023.2234554).
- [34] GROSSE C, OHTSU M, AGGELIS D, et al. *Acoustic emission testing: basics for research – applications in engineering.* 2. Switzerland: Springer; 2022. ISBN 978-3-030-67935-4
- [35] MAHMOUD H, MAZAL P, VLASIC F. Relationship between acoustic emission signal and loads on pneumatic cylinders. *Case Stud NondestrTest Eval.* 2020;35(2):222–238. ISSN 1058-9759. doi: [10.1080/10589759.2019.1662900](https://doi.org/10.1080/10589759.2019.1662900)
- [36] CHACON FERRANDO, Luis J, Artigao ANDICOBERRY E, et al. An experimental study on the applicability of acoustic emission for wind turbine gearbox health diagnosis. *J Low Frequency Noise Vib Active Control.* 2016;35(1):64–76. ISSN 1461-3484 doi: [10.1177/0263092316628401](https://doi.org/10.1177/0263092316628401)
- [37] JONES R. *A Guide to the interpretation of vibration frequency and time spectrums.* 1. USA: dr. Robert M Jones. 2011;1:23–31. ISBN 9781105036880.
- [38] MAIS J *Spectrum analysis: the key features of analyzing spectra.* 1. California, USA, 2002. Available at: https://cdn.skfmediahub.skf.com/api/public/0901d1968024acef/pdf_preview_medium/0901d1968024acef_pdf_preview_medium.pdf
- [39] FERNANDEZ A Typical bearing defects and spectral identification. online: power-mi. Available at: <https://power-mi.com/content/typical-bearing-defects-and-spectral-identification>
- [40] WIDODO A, YANG B-S, Eric YK, et al. Fault diagnosis of low speed bearing based on acoustic emission signal and multi-class relevance vector machine. *Case Stud NondestrTest Eval.* 2009;24(4):313–332. ISSN 1058-9759 doi: [10.1080/10589750802378974](https://doi.org/10.1080/10589750802378974)